APPLICATIONS OF
MODELLING AND SIMULATION
http://arqiipubl.com/ams eISSN 2600-8084 VOL 7, 2023, 156-167

Numerical Simulation of the Stress-Strain State of a Thin Plate in the ANSYS Package as a Two-Dimensional Formulation of the Thermo-Elasticity

Andry Sedelnikov, Valeria Serdakova, Aleksandra Nikolaeva and Maksim Evtushenko*

Samara National Research University, 443086, 34, Moscow Shosse, Samara, 443086, Russia

*Corresponding author: m.evtushenko.a@yandex.ru

Submitted 22 September 2023, Revised 19 October 2023, Accepted 30 October 2023, Available online 11 November 2023.

Abstract: This work considers numerical modeling of the stress-strain state of a homogeneous rectangular thin plate after a thermal shock. The presented solution is implemented in the finite element (FEM) package ANSYS Mechanical APDL 2020 R2. The task to be considered is a two-dimensional problem with the initial deflection of the plate. It is considered that the plate is cantilevered only at one end, but the other three edges are free. At the moment of a temperature shock, the plate acquires a curved shape. Within the framework of the heat conduction problem, two heat flows are taken into account. The first flow goes from the surface layer subjected to thermal shock deep into the plate. The second flow spreads parallel to its longitudinal axis. This axis is perpendicular to the plate embedding line. The dependencies of the temperature field of the plate are built. A comparative analysis was carried out with approximate analytical dependencies obtained in other works. The dependencies of the projections of the displacement vector of the plate points are obtained only in the case when the longitudinal displacement is small. There is also an analysis of the applicability of the results for practical purposes. For example, it is proposed to use the results obtained to assess the significance of the impact of thermal shock of solar panels on the motion of a small satellite.

Keywords: ANSYS package; Finite element method; Thermal shock; Thermo-elasticity problem; Stress-strain state.

1. INTRODUCTION

The studies of the phenomenon of thermo-elasticity begins in the early part of the last century. One of the first systematic presentations of the theory of unbonded thermo-elasticity for an isotropic body can be attributed to this period [1]. Some research related to the formulation and solution of the third initial-boundary task of heat conduction appeared in the middle of the 20th century. A work [2] could be taken as an example. It is one of the first papers describing the dynamic task of the theory of thermal tensions. The propagation of a one-dimensional thermoelastic wave in an elastic half-space is studied in this work. The wave is generated by a sudden heating of the plane, which limits the considered half-space.

The problems of calculating thermal tensions in flexible plates are considered in [3-5]. There are both thin plates without a heat-conducting layer and plates with a heat-conducting layer with a given temperature on their surface which could be studied. The problems were solved within linear formulations excluding the inertial terms of a non-linear nature. In works [6, 7], the temperature shock of semi-infinite bodies is studied. It is analyzed in view of the inertial terms necessary for the correct description of such rapidly dynamic phenomena as thermal shock. The advent and rapid development of space technology gave the task of temperature shock a new practical area. During its orbital motion, the spacecraft periodically falls into the shadow of the earth. This fact determines the advent of a temperature shock of the spacecraft solar panels when entering the shadow part of the orbit and leaving it [8-10]. Perturbations caused by the temperature shock can affect the motion parameters of a spacecraft [11-13]. Especially, when it comes to small spacecrafts, which are becoming more and more widespread nowadays. The exploitation of thin ROSA (Roll-out Solar Array) panels in experiments aboard the International Space Station showed the full significance of the temperature shock task [14-16]. Thermal oscillations turned out to be so intense that they did not allow ROSA to collapse at the end of the tests [14]. There are some studies confirming the decrease in the quality of target tasks performance by small spacecraft due to temperature shock [17-19]. This fact, first, concerns solving the task of remote sensing [20-22] and the implementation of gravity-sensitive experiments [23-27].

Thus, it is necessary to develop procedure accounting for the impact of temperature shock on the motion parameters of a spacecraft for the effective development of space technology, in particular, small spacecrafts. In [11], the structure of the method of such accounting is presented. The approximate dependencies of the projections of the displacement vector of points

of a thin plate under thermal for one-dimensional [28] and two-dimensional [29] models of thermo-elasticity have been reported in [28, 29].

The purpose of this study is to carry out numerical simulation of temperature shock and a comparative analysis of the results with the previously obtained approximate dependencies. This process will make it possible to reveal the area of application of the dependencies when considering the effect of temperature shock on the motion of a small satellite. Verification of approximate dependencies is very important for their application in the development of a small spacecraft. In this work, new results concerning the accuracy of approximate analytical dependencies have been obtained [28], [29]. Using the finite element method in the thermos-elasticity problem, various results of plate bending from a temperature shock with and without loss of stability were obtained [30].

2. SIMPLIFYING ASSUMPTIONS AND MATHEMATICAL MODEL

Let us consider the two-dimensional model of thermo-elasticity described in [29]. The main simplifying assumptions within this model are as follows [29]:

a) A thin homogeneous plate, rigidly fixed on one edge and free on the other three edges is considered.
b) At $t = 0$ (i.e., at the moment of thermal shock), the plate has a non-planar shape: $\vec{u}_0 = \left(0,0,u_{z0}(x,0)\right)$.
c) The heat flow is considered steady and stationary: $Q_0 = 1400$ W/m^2.
d) All physical properties of the plate material are homogeneous and the same in the considered temperature range.
e) When describing thermal conductivity, the Fourier law is valid.
f) The initial temperature of all points of the plate is the same and equal to: $T_0 = 200$ K.
g) The thickness of the plate is small compared to its other dimensions.
h) The heat transfer through the side surfaces of the plate is negligible.

With more accurate modeling, a number of simplifying assumptions can be abandoned. For example, the independence of thermophysical properties from temperature. However, in practice it is possible to use structural materials with constant thermophysical properties in a wide range of temperatures. Such materials include, for example, composite materials. Heat transfer through the side surfaces can be taken into account. However, for real solar panel designs, its value is about three orders of magnitude lower (and for ROSA panels about six orders of magnitude lower) than the heat transfer through the upper and lower surfaces of the plate.

The equations of the two-dimensional heat conduction model with the third boundary conditions and initial conditions are [29]:

$$\begin{cases} \dfrac{\partial T(x,\,z,\,t)}{\partial t} = a^2\left(\dfrac{\partial^2 T(x,\,z,\,t)}{\partial x^2} + \dfrac{\partial^2 T(x,\,z,\,t)}{\partial z^2}\right),\ 0 \le x \le l,\ 0 \le z \le h,\ t > 0; \\ \left(\lambda \dfrac{\partial T(x,\,h,\,t)}{\partial n}\right) = Q_0 \cdot \cos\left(\dfrac{du_{z0}(x,\,0)}{dx}\right) - e\Theta\left(T^4(x,\,h,\,t) - T_C^4\right),\ 0 \le x \le l, z = h,\ t > 0; \\ \left(\lambda \dfrac{\partial T(x,\,0,\,t)}{\partial n}\right) = -e\Theta\left(T^4(x,\,0,\,t) - T_C^4\right),\ 0 \le x \le l, z = 0,\ t > 0; \\ T(x,\,z,\,0) = T_0 = const. \end{cases} \tag{1}$$

where $T = T(x,z,t)$ is temperature of the plate, a is the diffusivity coefficient, λ is the thermal conductivity, $\vec{n}$ is the unit vector of the outer normal to the element of the plate surface, Q_0 is the maximum score of the external heat flux, e is emissivity of the plate material, Θ is the Stefan-Boltzmann constant, T_C is plate ambient temperature and l is the plate length.

The thermo-elasticity equations for various components of the plate spot displacement vector will have the form [29]:

$$\begin{cases} \dfrac{3(1-2\nu)}{2(1+\nu)}\dfrac{\partial^3 u_y(x,y,t)}{\partial x^3} + \dfrac{6\rho(1-\nu^2)}{Eh^2}\dfrac{\partial^2 u_y(x,y,t)}{\partial t^2} b = \dfrac{12(1-\nu^2)}{h^3}\alpha\int_0^h [T(x,\,z,\,t) - T_0]dz, \\ 0 \le x \le l,\ 0 \le y \le \dfrac{b}{2},\ t > 0; \\ D\dfrac{\partial^4 u_z(x,\,t)}{\partial x^4} + \rho h\dfrac{\partial^2 u_z(x,\,t)}{\partial t^2} = -2\mu\alpha\int_{-h/2}^{h/2}\left[2\dfrac{\partial T(x,z,\,t)}{\partial z} + z\dfrac{\partial^2 T(x,z,\,t)}{\partial z^2}\right]dz + \dfrac{\partial^2 u_{z0}(x,\,0)}{\partial x^2}\sigma_{xz}, \\ 0 \le x \le l,\ t > 0. \end{cases} \tag{2}$$

where μ is the Lame coefficient, σ_{xz} is a component of the stress tensor arising in the plate due to the initial deflection $u_{z0}(x,0)$ (Figure 1), h is the plate thickness, D is cylindrical bending stiffness of the plate, ρ is plate material density, E is the Young's modulus, b is plate width, α is linear expansion of the material and ν is Poisson's ratio.

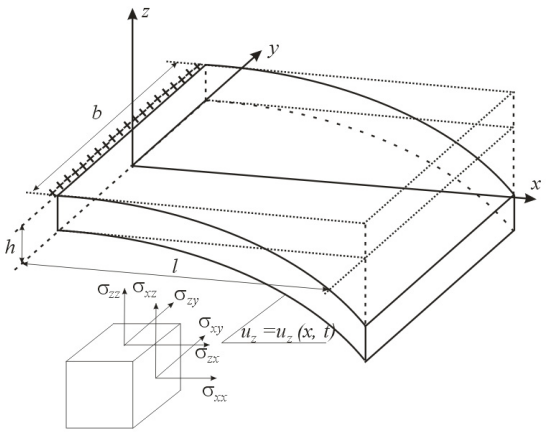

Figure 1. The shape of the plate and the stresses from its initial deflection at the moment of thermal shock [29]

Let us supplement this system with boundary and initial conditions [29]:

$$\begin{cases} u_y(0, y, t) = 0,\ x = 0,\ 0 \le y \le \dfrac{b}{2},\ t > 0; \\ \dfrac{\partial u_y(x,\ y,\ t)}{\partial x} = 0,\ x = 0,\ 0 \le y \le \dfrac{b}{2},\ t > 0. \end{cases} \tag{3}$$

$$\begin{cases} u_z(0,\ t) = 0,\ x = 0,\ t > 0; \\ \dfrac{\partial u_z(x,\ t)}{\partial x} = 0,\ x = 0,\ t > 0. \end{cases} \tag{4}$$

$$\begin{cases} \dfrac{\partial^2 u_y(x, y,\ t)}{\partial x^2} = 0,\ x = l,\ t > 0; \\ \dfrac{\partial^3 u_y(x, y,\ t)}{\partial x^3} = 0,\ x = l,\ t > 0. \end{cases} \tag{5}$$

$$\begin{cases} \dfrac{\partial^2 u_z(x,\ t)}{\partial x^2} = 0,\ x = l,\ t > 0; \\ \dfrac{\partial^3 u_z(x,\ t)}{\partial x^3} = 0,\ x = l,\ t > 0. \end{cases} \tag{6}$$

$$\begin{cases} u_y(x,\ y,\ 0) = 0,\ 0 \le x \le l,\ \ 0 \le y \le \dfrac{b}{2},\ t = 0; \\ u_z(x,\ 0) = u_{z0}(x,\ 0),\ 0 \le x \le l,\ \ t = 0. \end{cases} \tag{7}$$

The systems given in Equations (3) and (4) reflect the absence of displacements in the embedment and are geometric boundary conditions. On the other hand, the systems in Equations (5) and (6) determine the absence of internal forces on the free edge of the plate and are static. The system in Equation (7) shows the initial deformations in view of its initial deflection.

3. NUMERICAL SIMULATION

3.1 Numerical Values of the Main Parameters of the Model

For computational modeling, the values of the main characteristics of the plate as in [29] (Table 1) can be used. Thus, it is possible to make an adequate comparison of these results.

3.2 Building a Finite Element Model in the ANSYS Package

Simulation is realized in the ANSYS package. For the finite element representation of the plate, we will select an element of the SOLID226 type (Figure 2). It has twenty nodes. Each knot has six degrees of freedom. Figure 3 shows the interface for describing the properties of an element of type SOLID226. To use this element, the properties of elasticity, plasticity, viscoelasticity, viscoplasticity and creep must be set. Also, if necessary, the options of hyperelasticity, large deformation, large deflection and stiffening effects can be used.

To set external influences on the surface of an element of the SOLID226 type (Figure 2), the SURF152 element will be used. Its appearance is given in Figure 4. Figure 5 shows an interface for describing the element properties of type SURF152. Next, the properties of the plate material are set, and a geometric model is built (Figure 6). To obtain a finite element model, the parameters of the main mesh of finite elements are set (Figure 7). Next, the heat flux distributed along the length of the plate (W/m^2) and the initial deflection before thermal shock are set (Figure 8). Geometric boundary conditions (Equations (3)

and (4)) are also introduced at this stage. Thus, the construction of the finite element model of the plate in the ANSYS package has been completed.

Table 1. Characteristics of the plate

Parameter	Designation	Value	Dimension
Plate material	–	MA2	–
Coefficient of thermal conductivity	λ	96.3	W/(m.K)
Stefan-Boltzmann constant	Θ	5.67×10^{-8}	$W/(m^2.K^4)$
External heat flux	Q	1400	W/m^2
Ambient temperature	T_c	3	K
Initial temperature of the plate	$T_0 = T(z, 0)$	200	K
Degree of blackness	e	0.2	–
Specific heat	c	1130.4	J/(kg.K)
Density	ρ	1780	kg/m^3
Young's Module	E	4×10^{11}	Pa
Shift modulus	μ	1.6×10^{10}	Pa
Poisson's Ratio	v	0.3	–
Plate length	l	1	m
Plate width	b	0.5	m
Plate thickness	h	1	mm
Equation of the initial deflection of the plate	u_{z0}	$-0.1x^2$	m

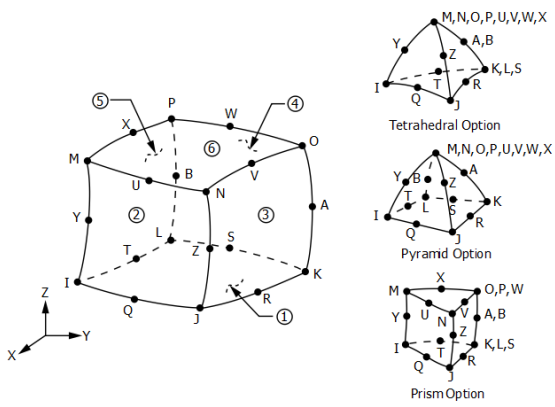

Figure 2. Schematic of an element of type SOLID226

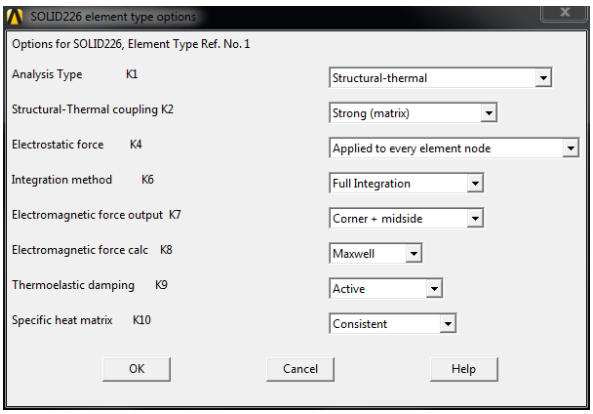

Figure 3. Setting properties of an element of type SOLID226

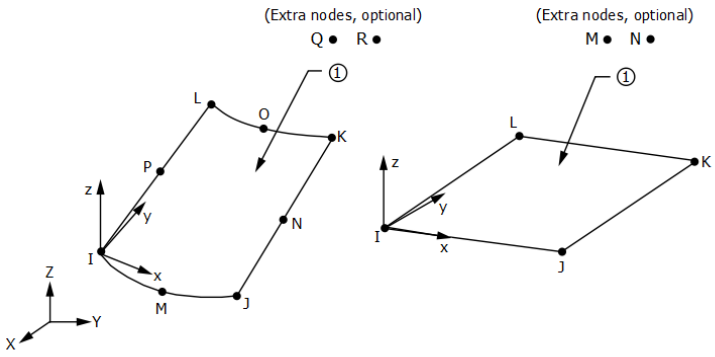

Figure 4. Scheme of the SURF152 type element

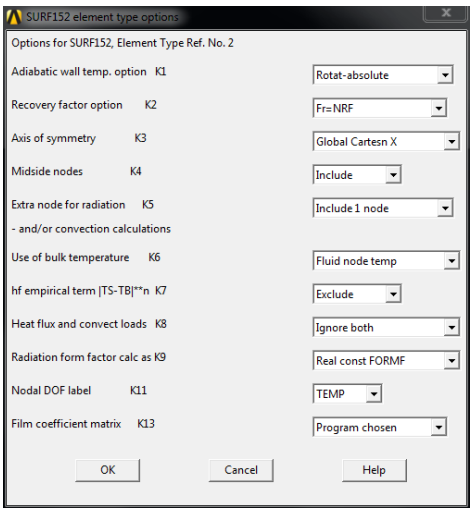

Figure 5. The element options of type SURF152

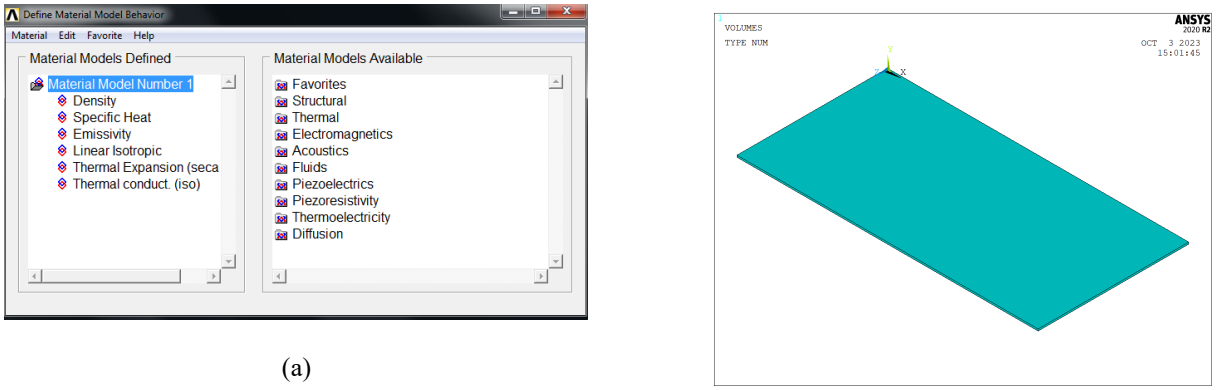

(a) (b)

Figure 6. Building a geometric model of a plate in the ANSYS package: (a) Panel for setting plate material properties; (b) View of the plate without heat flow

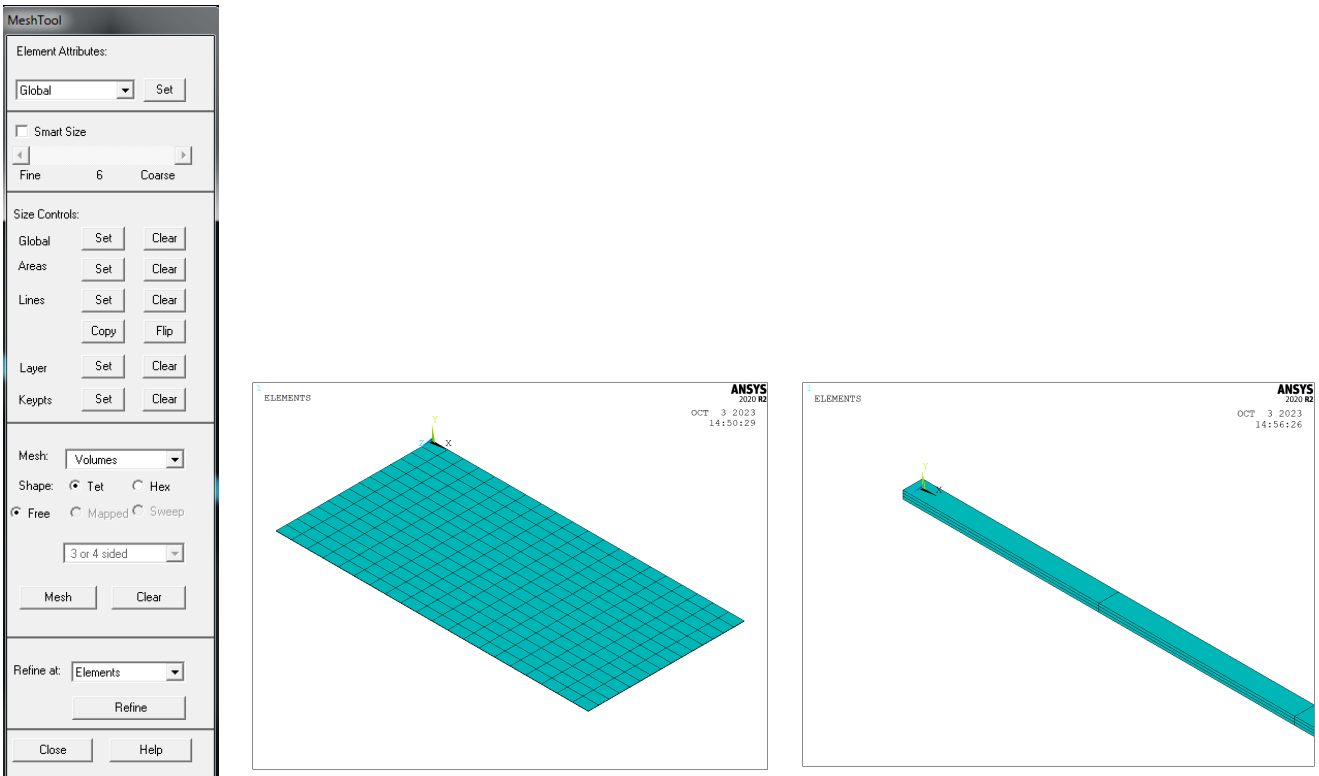

(a) (b) (c)

Figure 7. Building a finite element net in the ANSYS package: (a) Panel for setting grid parameters; (b) View of the plate with the grid; (c) A fragment of a three-layer plate with a grid

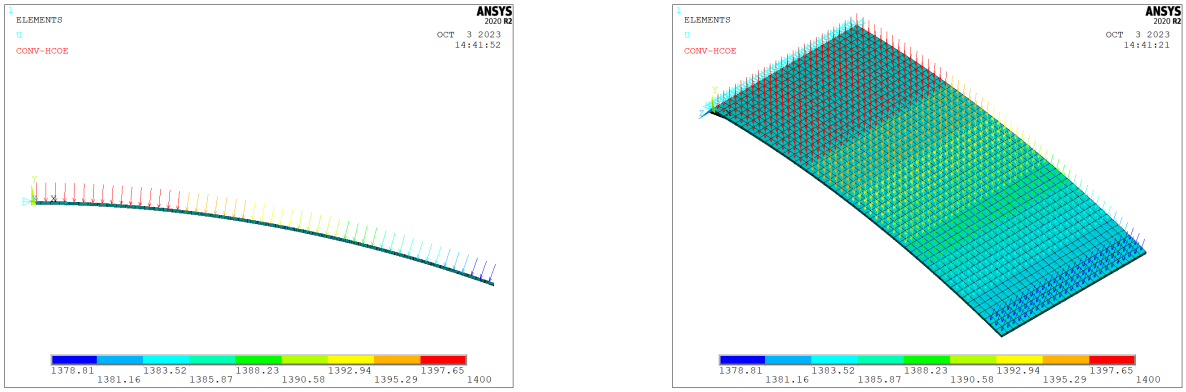

(a) (b)

Figure 8. View of a plate with a given heat flux in the ANSYS package: (a) Side view; (b) Axonometry

3.3. A Computational Experiment

There are two types of results obtained from the constructed model for the two-dimensional heat conduction model in the case of initial plate deflection. The first results are similar to the one-dimensional thermal conductivity model [28] and is characterized by a small initial deflection of the plate or softening of the rigid embedment boundary conditions (3) and (4), which allow the plate material to expand in the embedment (Figures 9 and 10).

Figure 11 gives the dependencies of the vector projections of displacements of the plate spots for fixing, corresponding to Figure 10. At small initial deflections, there are no significant differences in temperature fields for one-dimensional [28] and two-dimensional [29] models of thermal conductivity. Such differences are more clearly seen with significant initial deflections and simultaneous weakening of the boundary conditions in Equations (3) and (4) (Figure 10).

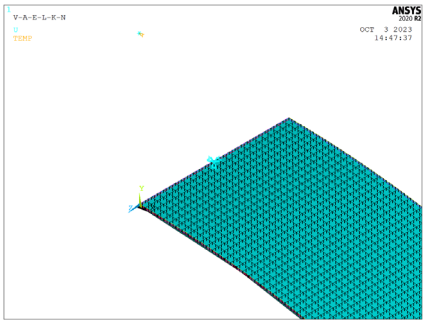

(a)

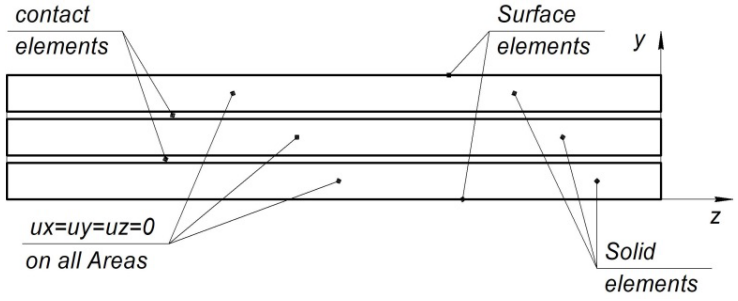

(b)

Figure 9. (a) A view of the plate with initial deflection in the ANSYS environment; (b) The scheme of rigid fastening of the plate layers in the embedment section, satisfying to the boundary conditions (Equations (3) and (4)).

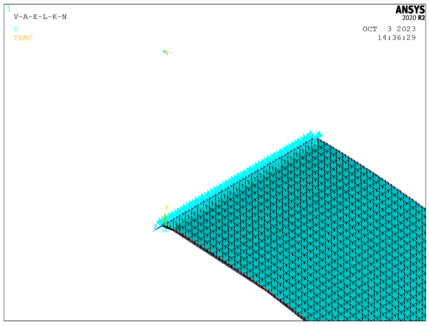

(a)

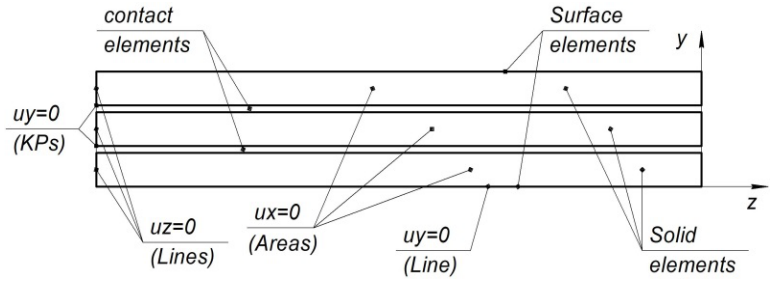

(b)

Figure 10. (a) A view of a plate with an initial deflection in the ANSYS environment; (b) The scheme of fixing the plate layers in the embedment section, corresponding to a softer fixation than boundary conditions (Equations (3) and (4))

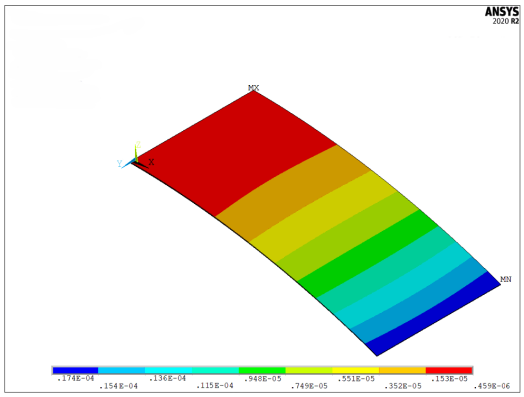

(a)

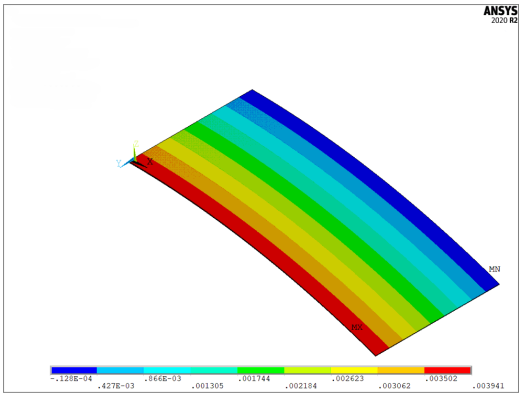

(b)

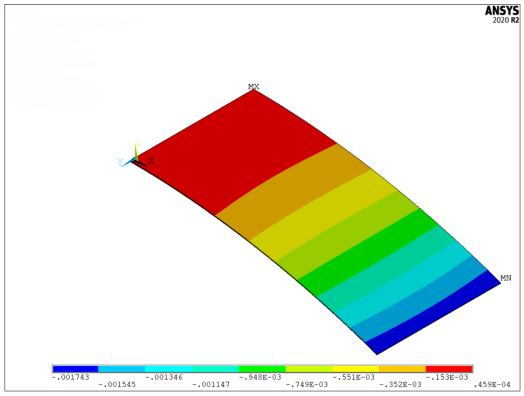

(c)

Figure 11. Projections of the displacement vector of plate points: (a) u_x; (b) u_y; (c) u_z

Figure 11 shows that u_x are smaller than u_z and u_y. This fact fully corresponds to the simplifications made in solving one-dimensional [28] and two-dimensional [29] heat conduction problems. In this case, the temperature values, as expected, turned out to be lower than for the one-dimensional problem due to less intense heating of the plate, which has an initial deflection. Figure 12 shows the temperature difference between the one-dimensional [28] and two-dimensional [29] models at the free end of the plate. Figure 12 shows the temperature difference between the one-dimensional [28] and two-dimensional [29] models at the free side of the plate ($x = l$) and in the plate middle ($x = l/2$). As expected, the smaller difference in heat fluxes in comparison with the one-dimensional model [28] in the plate middle contributed a smaller difference in the temperature dynamics within the different models. Thus, this type of result corresponds to the expected changes associated within of the initial deflection of the plate before the thermal shock.

The second type of results gives a more complex view of the stress-strain state of the plate during thermal shock. This type is common for cases of significant initial deflections and a model of rigid fastening corresponding to boundary conditions (3) and (4) (Figure 9). When such conditions are implemented within the framework of a computational experiment, the plate becomes unstable, which significantly complicates its stress-strain state. The dependencies of the displacement vector projections for this type of result are given in Figure 13.

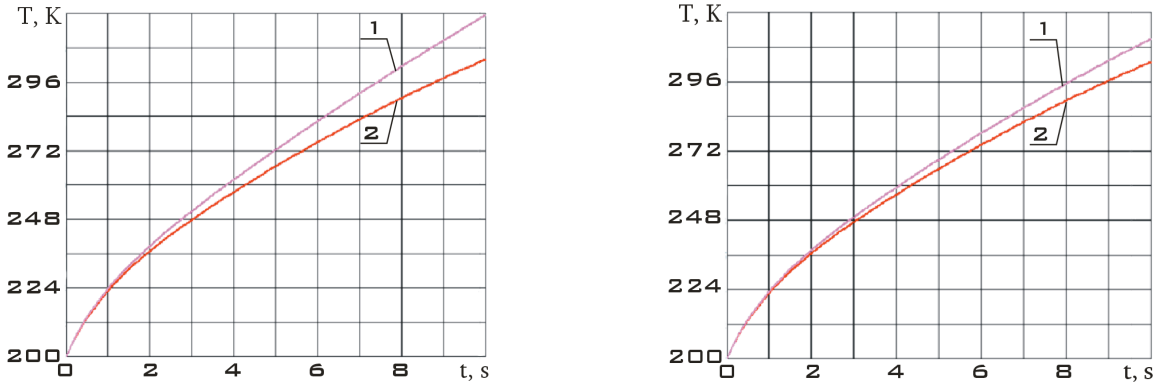

(a) (b)

Figure 12. Comparison of the temperature change of the upper layer of the plate subjected to thermal shock for: (a) $x=l$ (one-dimensional model); (b) $x = l/2$ (two-dimensional model). 1: Without a deflection, 2: With a deflection $u_{z0} = -0.1\,x^2/l^2$

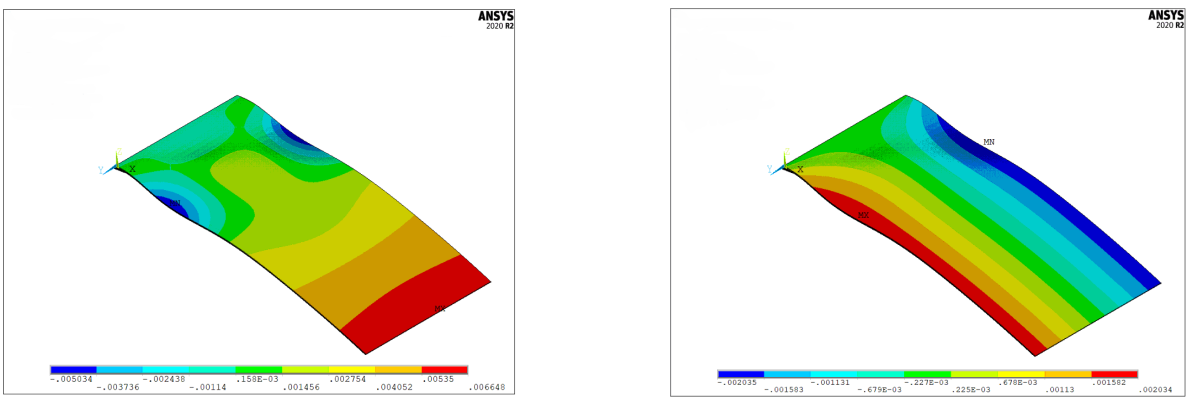

(a) (b)

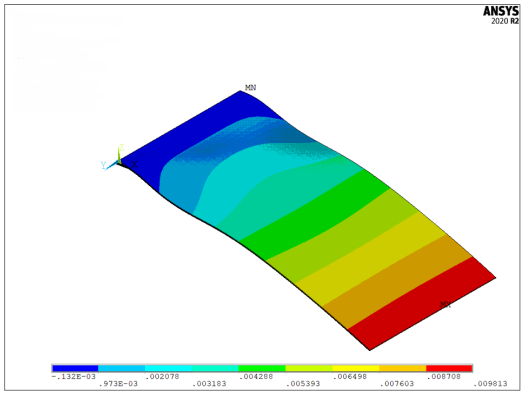

(c)

Figure 13. Projections of the displacement vector of plate points: (a) u_x; (b) u_y; (c) u_z

The studies carried out in [31] show that such a loss of stability occurs due to the excess of the sum of thermal stresses and stresses caused by the initial deflection, the critical stability stresses, which can be presented as:

$$\sigma_{cr} = K\frac{\pi^2 D}{b^2 h} \tag{8}$$

where K is the coefficient depending on plate fixation. Let us estimate the thermal tensions as suggested in [31]:

$$\sigma_{x(term)} = \frac{E}{1-\mu}\alpha\left(T(x,\,z,\,t)-T(x,\,z,\,0)\right) \tag{9}$$

Then full tensions σ_x within of the tensions from the initial deflection can be determined as:

$$\sigma_x = -E\left[\frac{1}{2(1+\mu)}\frac{\partial u_z}{\partial x}+\frac{\alpha}{1-\mu}\left(T(x,z,t)-T(x,z,0)\right)\right] \tag{10}$$

The estimates made in [31] show that for the simulated situation (Table 1), the assessment of critical tensions in Equation (8) gives:

$$\sigma_{cr} = K\frac{\pi^2 D}{b^2 h} = K\frac{\pi^2 E h^2}{12b^2(1-\nu^2)} \approx 1.6\ MPa \tag{11}$$

Using the expression for the initial deflection of the plate by the law: $u_z(0,t) = -0.1x^2$ and the values of the main parameters from Table 1, we have from (10) [31]:

$$\sigma_{xz} = -E\frac{1}{2(1+\mu)}\left.\frac{\partial u_z}{\partial x}\right|_{x=0.5} \approx 1.5\ MPa \tag{12}$$

Equation (12) gives an estimate of the maximum tensions from the initial deflection. The dependence of thermal tensions on time corresponding to different types of fastening (Figures 9 and 10) is shown in Figure 14 [31]. In accordance with Equation (10), thermal tensions (Figure 14) are added to the tensions from the initial deflection (12). This sum may exceed the critical values (11). This leads to the loss of stability shown in Figure 13. In practice, loss of stability should be avoided. Equation (11) can be used for approximate estimation of critical tensions.

3.4. Analysing the Results of Computational Experiments of the Second Type

It should be noted that when stability is lost, the two-dimensional formulation of the heat conduction problem becomes incorrect. The use of approximate analytical dependences obtained for one-dimensional [28] and two-dimensional [29] models of thermal conductivity can lead to erroneous results. This is explained by the fact that buckling of the plate as a result of the loss of stability will lead to a more complex temperature field of the surface layer than is described in the framework of one-dimensional and two-dimensional thermal conductivity models. A correct description will require a three-dimensional formulation and separate studies of the dynamics of plate buckling during this process. The study of such situation is interesting only from a theoretical point of view since in practice the loss of stability is an unacceptable phenomenon. It will lead, for example, to a decrease in the efficiency of the solar battery panel of the spacecraft [31] or the appearance of undesirable additional perturbations of its motion [29, 31]. As shown by the computational experiment, this phenomenon can be eliminated by weakening the rigidity of the plate fastening unit. Therefore, a deeper analysis of data of this type was not carried out in this work, since it requires separate studies and a transition from a two-dimensional to a three-dimensional model of thermal conductivity.

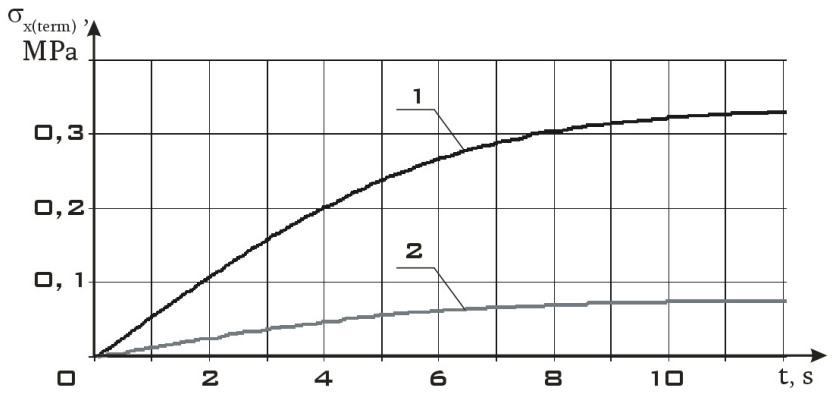

Figure 14. Dependence of thermal tensions arising from thermal shock, on time. 1: For the case of fixing the elastic element corresponding to Figure 9, 2: for the case of fixing the elastic element corresponding to Figure 10

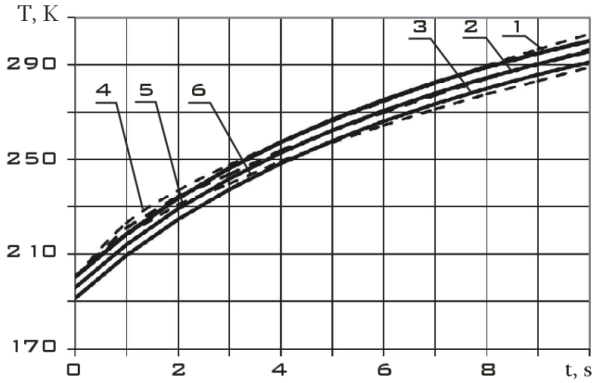

Figure 15. The temperature change of the surface plate layer at the initial deflection law $u_{z0} = -0.1\,x^2/l^2$ obtained using numerical experiment. 1: Near the termination *(x ≈ 0)*; 2: In the middle of the plate *(x ≈ l/2)*; 3: On the free edge of the plate *(x ≈ l)* according to Equation (13) at C = 200 K/m, a = 1 s and M = 3 K/m; 4: Near the termination *(x ≈ 0)*; 5: In the middle of the plate *(x ≈ l/2);* 6: On the free edge of the plate *(x ≈ l)*

3.5. Comparison of the Results of Computational Experiments with Approximate Analytical Dependencies

Let us return to the results of the first type and compare them with approximate analytical solutions for the projections of the displacement vector and the temperature field [28, 29]. In [29], the temperature field was approximated as follows.

$$T(x,\,z,\,t) = Cz\frac{t}{t+a} - Mx + T_0,\; 0 \le x \le l,\; 0 \le z \le h,\;\; t > 0 \tag{13}$$

where m, C and a are constants. Taking the constant M = 3 K/m, the temperature field can be obtained using an approximate solution (Figure 15) [29]. Figure 15 shows good convergence of the result of the approximate analytical dependence of the temperature field with the computational experiment. Especially on the interval [3, 10] s. The only drawback in Equation (13) seems to be the impossibility of realizing a uniform temperature field at the initial moment of time. Thus, Equation (13) does not satisfy the initial condition of the system (1). However, over time, this drawback is eliminated due to uneven heating of the plate layers as a result of thermal shock. Convergence can be improved by complicating dependence. However, this will entail a significant complication of the search for approximate solutions similar to those presented in [28, 29].

The dependences of the deflections of the end section of the plate ($x = 1$), obtained from the results of the computational experiment and from the approximate analytical dependences given in [28] and [29] are shown in Figure 16. As can be seen from Figure 16, good convergence of deflections is observed throughout the entire time interval. It worsens slightly on the interval [0, 3] s due to differences in the temperature field (Figure 15) in this time interval. Let us consider the second projection of the displacement vector $u_y(x, y, t)$. Figure 17 shows the dependency $u_y = u_y(x, b/2, t)$.

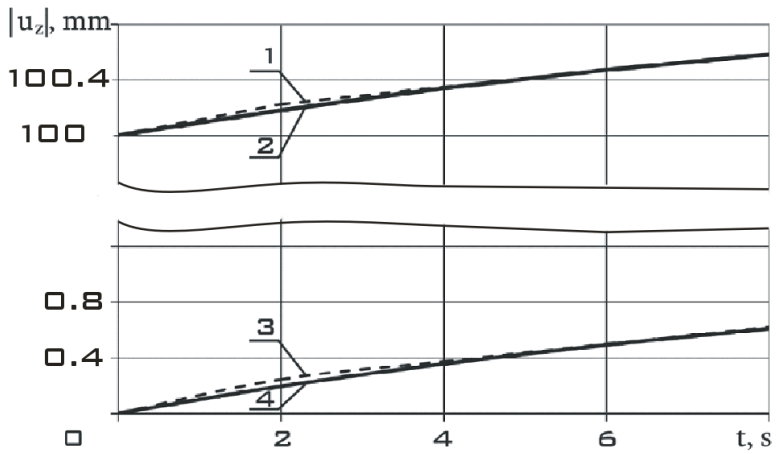

Figure 16. Dynamics of deflections u_z end section of the plate *(x = l)* at initial deflection $u_{z0} = -0.1\,x^2/l^2$. 1: According to the computational experiment, 2: Using approximate dependence [29] without initial deflection, 3: According to the computational experiment, 4: According to the approximate dependence [28]

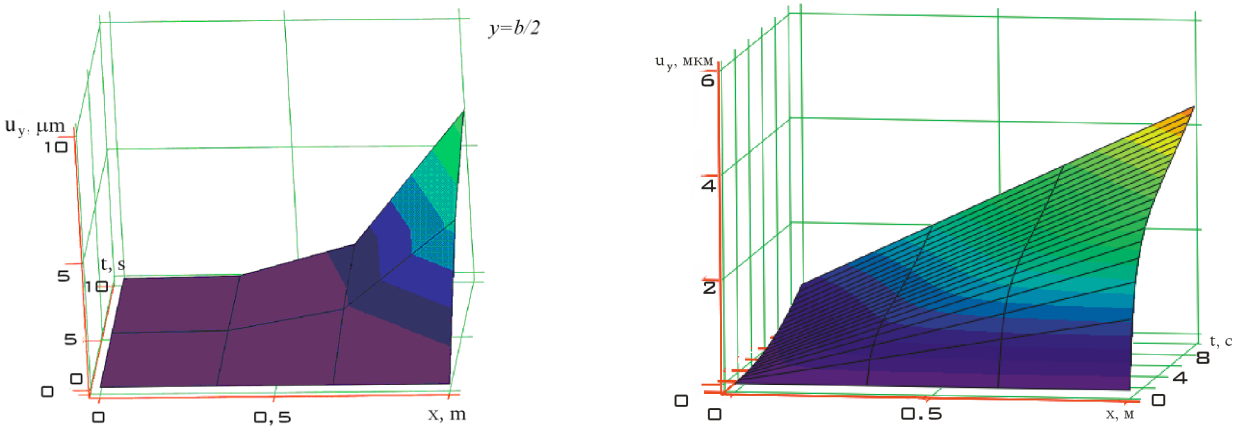

(a) (b)

Figure 17. The dependency $u_y(x, y, t)$ for $u_y(x, y = b/2, t)$, corresponding to approximate dependencies [18]: (a) one-dimensional model) and [19]; (b) two-dimensional model

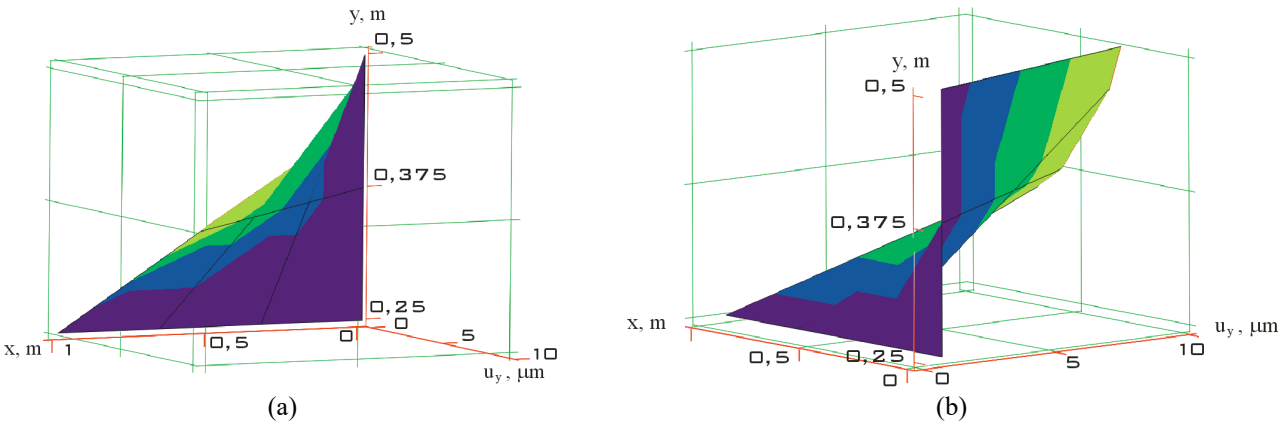

(a) (b)

Figure 18. The dependency $u_y(x, y, t)$ for $u_y(x, y, t = 1)$: (a) $u_y(x, y, t = 5)$; (b) Corresponding to approximate dependencies [19] (two-dimensional model)

The surface in Figure 17(b) is smoother than in Figure 17(a). This is an advantage of the two-dimensional model. However, in this case, the boundary conditions (3) are broken, according to which $u_y(0, y, t)$. This is clearly seen in Figure 17(b). The boundary condition (3) is satisfied only for small values of t (Figure 18).

Comparison of the results of a computational experiment (Figure 11(b)) and calculations based on approximate dependencies [28] and [29] does not demonstrate good agreement. This is due to the simple view of the function itself $u_y(x, y, t)$ with the obtaining approximate dependence's [28] and [29]. A more correct description is possible only in the framework of the three-dimensional formulation of the heat conduction problem. It can only be noted that dependence (Figure 17(b)) within of the two-dimensional model agrees better with the computational experiment than dependence (Figure 17(a)) within of the one-dimensional model. This may not be due to the improvement of the dependence type $u_y(x, y, t)$ in the two-dimensional model [29] compared to the one-dimensional model [28]. Since the boundary conditions (3) were broken in the computational experiment.

4. CONCLUSION

Thus, within the framework of a two-dimensional model, it was possible to describe the temperature field using the approximate dependence Equation (13), to show the convergence of deflections obtained using approximate dependences with the results of a computational experiment. However, it was not possible to greatly improve the presentation of u_y projection of the displacement vector in the two-dimensional formulation of the thermos-elasticity problem. For such an improvement, it is necessary to significantly complicate the approximating dependencies.

From the point of view of practical application, this drawback is insignificant. The main displacement of the spots of the plate during thermal shock is the deflection. It is quite accurately described using approximate dependencies within of a two-dimensional model. At zero initial deflection, the two-dimensional model degenerates into a one-dimensional one. It should be noted that as a result of the computational experiment, cases of plate stability loss were identified. These cases were analyzed, but excluded from consideration, since they require a more complex three-dimensional formulation of the heat conduction problem.

Thus, the performed computational experiment confirmed the correctness of the approximate analytical dependencies for the deflections of the plate points obtained in [28] and [29]. They can be used for practical calculations. For example, when assessing the impact of temperature shock on the motion of the movement of a small spacecraft. In theoretical studies of the stress-strain state of a plate after a thermal shock, it should be noted that in the framework of a two-dimensional formulation, apparently, it was not possible to achieve significant improvements in the description. Even in its relatively simple representation, the satisfaction of all boundary and initial conditions by the obtained approximate solution [29] was not achieved. Therefore, the convergence of the results with the computational experiment is not satisfactory.

ACKNOWLEDGMENT AND FUNDING

This work is supported by the Ministry of education and science of the Russian Federation in the framework of the State Assignments to higher education institutions and research organizations in the field of scientific activity (the project FSSS-2023-0007).

DECLARATION OF CONFLICTING INTERESTS

The authors declare no potential conflicts of interest with respect to the research and publication of this article.

REFERENCES

[1] N. N. Lebedev, Temperature Stresses in the Theory of Elasticity 1937, Moskow- Leningrad: ONTI.
[2] V. I. Danilovskaya, Temperature stresses in an elastic half-space arising due to sudden heating of its boundary, *Applied Mathematics and Mechanics*, 14(3), 1950, 316-318.
[3] E. Melan and H. Parkus, Wärmespannungen inflolge stationärer temperaturfelder 1953, Wien: Springer-Verlag.
[4] Parkus, H. Thermal stresses in bodies with random surface temperature, *ZAMM*, 42, 1962, 499-507.
[5] R. D. Mindlin and H. L. Cooper, Thermoelastic stress around a cylindrical inclusion of elliptic cross section, *Journal Applied Mechanics*, 17, 1950, 265-270.
[6] E. M. Kartashov, New model ideas in dynamic thermoviscoelasticity in the problem of thermal shock, *Doklady Mathematics*, 86(2), 2012, 704-706.
[7] E. M. Kartashov, New model representations of dynamic thermoviscoelasticity in the problem of heat shock, *Journal of Engineering Physics and Thermophysics* 85(5), 2012, 1102-1113.
[8] A. V. Sedelnikov and D. I. Orlov, Analysis of the significance of the influence of various components of the disturbance from a temperature shock on the level of microaccelerations in the internal environment of a small spacecraft, *Microgravity Science and Technology*, 33(2), 2021, 22.
[9] D. I. Orlov, Modeling the temperature shock impact on the movement of a small technological spacecraft, *AIP Conference Proceedings*, 2340(1), 2021, 050001.
[10] Z. Shen and G. Hu, Thermally induced dynamics of a spinning spacecraft with an axial flexible boom, *Journal of Spacecraft and Rockets,* 52(5), 2015, 1-6.
[11] A. V. Sedelnikov, V. V. Serdakova and A. S. Nikolaeva, Method of taking into account influence of thermal shock on dynamics of small satellite and its use in analysis of microaccelerations, *Microgravity Science and Technology*, 35(3), 2023, 25.
[12] Z. Shen, S. Hao and H. Li, Thermoviscoelastic dynamics of composite thin-walled booms on spacecrafts subjected to solar radiation, *Composite Structures*, 294(7-8), 2022, 115795.

[13] P. A. Lyukshin, N. Y. Matolygina, S. V. Panin and B. A. Lyukshin, Strength analysis of anisotropic thermal barrier coating under heat shock, *Procedia Engineering*, 113, 2015, 408-412.
[14] M. K. Chamberlain, S. H. Kiefer, M. LaPointe and P. LaCorte, On-orbit flight testing of the roll-out solar array, *Acta Astronautica*, 179, 2021, 407-414.
[15] M. K. Chamberlain, S. H. Kiefer and J. A. Banik, On-orbit structural dynamics performance of the roll-out solar array, *Proceedings of the AIAA Spacecraft Structures Conference*, Kissimmee, USA, 2018, 1-9.
[16] B. R. Spence, S. White, M. LaPointe, et al., International space station (ISS) roll-out solar array (rosa) spaceflight experiment mission and results, *IEEE 7th World Conference on Photovoltaic Energy Conversion (WCPEC)*, Waikoloa Village, HI, 2018, 3522-3529.
[17] J. D. Johnston and E. A. Thornton, Thermal response of radiantly heated spinning spacecraft booms, *Journal of Thermophysics and Heat Transfer*, 10(1), 1996, 60-68.
[18] A. V. Sedelnikov, D. I Orlov, V. V. Serdakova and A. S. Nikolaeva, The Symmetric formulation of the temperature shock problem for a small spacecraft with two elastic elements, *Symmetry*, 15(1), 2023, 172.
[19] Z. Shen and G. Hu, Thermally induced vibrations of solar panel and their coupling with satellite, *International Journal of Applied Mechanics*, 5(3), 2013, 50031.
[20] J. D. Johnston and E. A. Thornton, Thermally induced attitude dynamics of a spacecraft with a flexible appendage, *Journal of Guidance, Control and Dynamics*, 4, 1998, 581-587.
[21] V. I. Abrashkin, Y. Y. Puzin, A. S. Filippov, et al., Detection of the rotational motion of the Aist-2D small spacecraft by magnetic measurements. *Cosmic Research*, 57(1), 2019, 48-60.
[22] R. Akhmetov, A. Filatov, R. Khalilov, et al., AIST-2D: Results of flight tests and application of earth remote sensing data for solving thematic problems, *The Egyptian Journal of Remote Sensing and Space Science*, 26(3), 2023, 427-454.
[23] A. Wang, S. Wang, H. Xia and G. Ma, Dynamic *Modeling and Control for a Double-State Microgravity Vibration Isolation System*, *Microgravity Science and Technology*, 35(1), 2023, 9.
[24] W. Liu, Y. Zhang, Z. Li and W. Dong, Control performance simulation and tests for microgravity active vibration isolation system onboard the Tianzhou-1 cargo spacecraft, *Astrodynamics*, 2(12), 2018, 1-22.
[25] Q. Kang and W. R. Hu, Microgravity experimental satellite SJ-10, *Bulletin Chinese Academy of Science*, 31(5), 2016, 574-580.
[26] J. Zhang, W. Dong and Z. Wang, Development of a New microgravity experiment facility with electromagnetic launch, *Microgravity Science and Technology*, 33(6), 2021, 68.
[27] A. S. Taneeva, The formation of the target function in the design of a small spacecraft for technological purposes, *Journal of Physics: Conference Series*, 1901(1), 2021, 012026.
[28] A. V. Sedelnikov, D. I. Orlov, V. V. Serdakova and A. S. Nikolaeva, Investigation of the stress-strain state of a rectangular plate after a temperature shock, *Mathematics*, 11(3), 2023, 638.
[29] A. V. Sedelnikov, D. I. Orlov, V. V. Serdakova and A. S. Nikolaeva, Investigating the temperature shock of a plate in the framework of a static two-dimensional formulation of the thermoelasticity problem, *Aerospace*, 10(5), 2023, 445.
[30] H. L. Ton-That, A combined strain element to functionally graded structures in thermal environment, *Acta Polytechnica*, 60(6), 2020, 528-539
[31] A. V. Sedelnikov, V. V, Serdakova, D. I. Orlov, A. S. Nikolaeva and M. A. Evtushenko, Modeling the effect of a temperature shock on the rotational motion of a small spacecraft, considering the possible loss of large elastic elements stability, *Microgravity Science and Technology*, 34(4), 2022, 78.